Inorganic Chemistry
Article

Inorg. Chem. **2009**, *48*, 11265–11276 **11265**
DOI: 10.1021/ic901749r

Ligand-Based Modification of the Structures and Optical Properties of New Silver(I)-Rhenate(VII) Oxide/Organic Hybrid Solids

Haisheng Lin, Xiaomeng Wu, and Paul A. Maggard*

Department of Chemistry, North Carolina State University, Raleigh North Carolina 27695-8204

Received September 3, 2009

A new series of silver(I)-rhenate(VII) hybrids was systematically prepared under hydrothermal conditions from eight different N-donor organic ligands (isonicotinate=inca, pyrazine-2-carboxylate=pzc, 1,2,4-triazole=tro, pyridazine=pda, 4,4′-bipyridine=bpy, 1,2-bis(4-pyridyl)-ethane=dpa, 2,3-bis(2-pyridyl)pyrazine=bpp, and tetra-2-pyridinylpyrazine = tpp), and their resulting structures and optical properties were investigated. The reactions targeted a 1:1 molar ratio of Ag/Re, and new hybrid solids were prepared with the compositions $Ag(bpp)ReO_4$ (**1**), $Ag(tpp)ReO_4 \cdot H_2O$ (**2**), $Ag(Hinca)_2ReO_4 \cdot H_2O$ (**3**), $Ag(tro)ReO_4$ (**4**), $Ag(pda)ReO_4 \cdot 1/2H_2O$ (**5**), $Ag(Hpzc)ReO_4$ (**6**), $Ag_2(Hpzc)(pzc)(H_2O)ReO_4$ (**7**), $Ag(bpy)ReO_4$ (**8**), and $Ag(dpa)_2ReO_4$ (**9**). Hybrid solids **1**, **2**, and **3** each exhibit low-dimensional structures, consisting of $[Ag_2(bpp)_4]^{2+}$ and $[Ag_2(Hinca)_4]^{2+}$ dimers in **1** and **3**, respectively, and $[Ag(tpp)]_n^{n+}$ chains in **2**. Hybrid solids **4** and **5** contain a $[Ag(tro)]^+$ chain and a $[Ag_3(pda)_3]^{3+}$ cyclic trimer, respectively, that are both ReO_4-bridged into layered structures. Both **6** and **8** consist of ligand-pillared "$AgReO_4$" layers, while **7** is a Re-deficient analogue of **6** that contains ligand-pillared $[Ag_2(H_2O)ReO_4]^+$ layers where H_2O replaces the missing ReO_4^- anion. The hybrid networks of **8** and **9** are interpenetrating, owing to the length of the bpy and dpa ligands, and consist of bpy-pillared "$AgReO_4$" layers and ReO_4-filled $[Ag(dpa)_2]^+$ diamond-type networks that are 2-fold and 6-fold interpenetrating, respectively. Their optical properties and thermal stabilities were investigated using UV−vis transmittance, X-ray photoelectron spectroscopy, and thermogravimetric analysis. The measured properties were analyzed with respect to the varying structural modifications. The Ag−ReO_4 network dimensionalities, Ag coordination environments, and the ligand lengths and geometries are found to play important roles in the absorption coefficients, bandgap sizes, and whether the structure collapses softly to give condensed $AgReO_4$, respectively.

Introduction

The optical properties of heterometallic oxides that include both an early and a late transition metal have attracted growing interest owing to their relatively small bandgap sizes and potential uses in efficiently harvesting solar energy.[1] In particular, metal-oxides containing a d^{10} electron configuration (e.g., Cu^+, Ag^+) in combination with a d^0 transition-metal cation (e.g., Re^{7+}, W^{6+}, Nb^{5+}) have recently been investigated for their optical properties and for use as photocatalytic materials.[2−6] Owing to a Metal-to-Metal Charge Transfer (MMCT) excitation between the electron-donating d^{10} and electron-accepting d^0 configurations,[2] the bandgap sizes of these solids occur ∼0.5−1.5 eV lower than that of the alkali-metal analogues which have only a d^0 metal cation (e.g., $AgNbO_3$ versus $NaNbO_3$). For example, $AgNbO_3$,[2a] Ag_2MoO_4,[2b] $AgVO_3$, and Ag_3VO_4[2c] exhibit band-edge absorption in the visible part of the spectrum and have been investigated for use as visible-light photocatalysts for the production of H_2/O_2 from water under visible light. However, their synthetic preparation has proceeded primarily by conventional solid-state methods. There is therefore a severely restricted ability to investigate new structural or particle modifications to more deeply understand and tune their optical properties.

Solution-based hydrothermal synthetic techniques have enabled the incorporation of varying N-donor ligands as flexible structural components within metal-oxide frameworks, that is, as metal-oxide/organic hybrid solids.[7] This synthetic approach has yielded an immense structural diversity and a growing ability to tune physical properties expressed in

*To whom correspondence should be addressed. E-mail: paul_maggard@ncsu.edu. Phone: (+1) 919-515-3616. Fax: (+1) 919-515-5079.

(1) (a) Osterloh, F. E. *Chem. Mater.* **2008**, *20*(1), 35. (b) Han, H.; Frei, H. *J. Phys. Chem. C* **2008**, *112*(22), 8391. (c) Kudo, A.; Miseki, Y. *Chem. Soc. Rev.* **2009**, *38*, 253.

(2) (a) Kato, H.; Kobayashi, H.; Kudo, A. *J. Phys. Chem. B* **2002**, *106*, 12441. (b) Kato, H.; Matsudo, N.; Kudo, A. *Chem. Lett.* **2004**, *33*, 1216. (c) Konta, R.; Kato, H.; Kobayashi, H.; Kudo, A. *Phys. Chem. Chem. Phys.* **2003**, *5*, 3061.

(3) Kim, H. G.; Hwang, D. W.; Lee, J. S. *J. Am. Chem. Soc.* **2004**, *126*, 8912.

(4) Tang, J.; Zou, Z.; Ye, J. *J. Phys. Chem. B* **2003**, *107*, 14265.

(5) Mikhailova, D.; Ehrenberg, H.; Fuess, H. *J. Solid State Chem.* **2006**, *179*, 2004.

(6) Blasse, G. *Struct. Bonding* (*Berlin*) **1991**, *76*, 153.

(7) Hagrman, P. J.; Hagrman, D.; Zubieta, J. *Angew. Chem., Int. Ed.* **1999**, *38*, 2638.

Published on Web 11/03/2009

metal oxides.[8−14] The ligands function in a variety of roles to direct the structural arrangement, including as (1) charge-compensating cations, (2) bridging or terminating ligands coordinated to the metal sites, and (3) altering the local coordination environments. Thus, these methods can be used to alter a metal-oxide network and can serve as a gateway to more deeply probing the properties of heterometallic oxides. However, even with the identification of the "building blocks" in solution, there still exists substantial challenges in predicting their structures and resultant properties owing to the numerous possible arrangements of three-dimensional structures. While many relatively small advances have been reported, it is rare when a large and diverse set of ligands is utilized to unravel the effects of synthetic conditions, coordination preferences, and ligand geometries.[15]

Our current research efforts have significantly expanded the known structural diversity of hybrid solids containing a combination of d^0 with d^{10} transition metals,[16−22] and which we have used to modify their bandgap sizes and photocatalytic reactivities. Recent research shows that, for example, "$MReO_4$" (M = Ag^+ or Cu^+) layers derived from parent $MReO_4$ phases can be pillared by bridging or metal-coordinated ligands, leading to new hybrid metal-oxide/organic structures including $M(pyz)ReO_4$ (M = Cu, Ag),[16,17] $Cu(pzc)_2(H_2O)_2ReO_4$,[18] $M(pzc)_2(H_2O)_2AgReO_4$ (M = Co, Ni),[19] and $Cu(pzc)_2AgReO_4$.[20] The latter two examples can reversibly absorb interlayer water and consist of a chiral network, respectively. Hybrid solids in these systems can also undergo subsequent ligand-mediated structural transformations, such as for $Cu(bpy)ReO_4$ and $Cu(bpy)_2ReO_4 \cdot 1/2H_2O$,[21] and that are accompanied by a significant modulation of their bandgap sizes. Further, some of the first reported to exhibit photocatalytic activity were recently found in the related hybrid vanadates $[Ag(L)]_4V_4O_{12} \cdot xH_2O$ (L = bpy, $x = 2$; L = dpa, $x = 4$) and $Ag_4(pzc)_2V_2O_6$.[22] However, these investigations have been primarily based on only two or three different ligands.

Scheme 1. A Series of Selected N−Donor Organic Ligands Used in the Synthesis of New Silver(I)−Rhenate(VII) Hybrid Solids and Their Different Coordination Modes to Ag

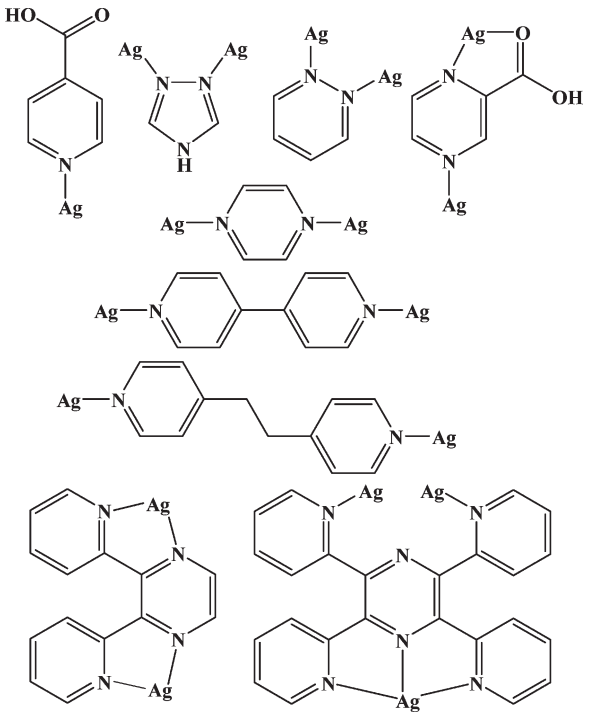

Herein, a diverse and systematic investigation of Ag(I)−Re(VII) hybrid structures (at a Ag/Re molar ratio of 1:1) was carried out using a series of eight different ligands, shown in Scheme 1, with varying lengths and geometric arrangement of N-donor atoms. The underlying emphasis is to more deeply probe the structural origins of their charge-transfer absorptions, modulation of bandgap sizes, as well as optical absorption coefficients. The hybrids were characterized structurally via X-ray diffraction, and their properties investigated using UV−vis transmittance, X-ray photoelectron spectroscopy, and thermogravimetric analysis. The nine new hybrids were analyzed for the effect of the ligand on both their structures and their properties, in order to reveal the roles of the Ag coordination environments, $Ag-ReO_4$ network dimensionalities, and ligand lengths and geometries.

Experimental Section

General Procedures. All starting materials were purchased commercially and used without further purification. Hydrothermal conditions were used to synthesize each hybrid solid, which involved heat sealing the starting materials and solvent inside an FEP Teflon pouch (3″ × 4″). A reagent amount of deionized water was used as the solvent in each of the reactions. The pouch was then placed inside a 125 mL Teflon-lined stainless steel reaction vessel that was backfilled with ~40 mL (~33%) of deionized water before closing. After holding the reaction at a fixed temperature (120 °C for 3 days for hybrids **1**−**7** and **9**; 140 °C for 3 days for **8**), it was then slowly cooled to room temperature at a rate of 6 °C h^{-1}. The resulting products were filtered, washed with deionized water, and dried and weighed in air. The phase purity of each hybrid was >95% according to powder X-ray diffraction data (see Supporting Information, Figure 1S).

(8) Cheetham, A. M. *Science* **1994**, *264*, 794.
(9) Pope, M. T.; Müller, A. *Angew. Chem., Int. Ed. Engl.* **1991**, *30*, 34.
(10) (a) Xu, L.; Qin, C.; Wang, X. L.; Wei, Y. G.; Wang, E. B. *Inorg. Chem.* **2003**, *42*, 7342. (b) Müller, A.; Reuter, H.; Dillinger, S. *Angew. Chem., Int. Ed. Engl.* **1995**, *34*, 2328.
(11) (a) Yaghi, O. M. *Nature* **1999**, *402*, 276. (b) Yaghi, O. M. *J. Am. Chem. Soc.* **1998**, *120*, 8571.
(12) Yan, B.; Maggard P. A. *Inorganic Chemistry in Focus III*; Meyer, G., Naumann, D., Weseman, L., Eds.; Wiley-VCH: Weinheim, 2006; Vol. *17*, pp 251−266.
(13) (a) Zheng, L.; Wang, X.; Wang, Y.; Jacobson, A. J. *J. Mater. Chem.* **2001**, *11*, 1100. (b) Zhang, C.; Liu, S.; Xie, L.; Gao, B; Sun, C.; Li, D. *J. Mol. Struct.* **2005**, *753*, 40.
(14) (a) Hagrman, D. E.; Zubieta, J. *J. Solid State Chem.* **2000**, *152*, 141. (b) LaDuca, R. L.; Finn, R.; Zubieta, J. *Chem. Commun.* **1999**, 1669. (c) Hagrman, P. J.; Finn, R. C.; Zubieta, J. *Solid State Sci.* **2001**, *3*, 745.
(15) (a) Eddaoudi, M.; Kim, J.; Wachter, J. B.; Chae, H. K.; O'Keeffe, M.; Yaghi, O. M. *J. Am. Chem. Soc.* **2001**, *123*, 4368. (b) Sun, D.; Cao, R.; Liang, Y.; Shi, Q.; Hong, M. *J. Chem. Soc., Dalton Trans.* **2002**, 1847. (c) Kitagawa, S.; Kitaura, R.; Noro, S. *Angew. Chem., Int. Ed.* **2004**, *43*, 2334. (d) Zeng, M. H.; Zhang, W. X.; Sun, X. Z.; Chen, X. M. *Angew. Chem., Int. Ed.* **2005**, *44*, 3079. (e) Liu, G.-X.; Huang, Y.-Q.; Chu, Q.; Okamura, T.-A.; Sun, W.-Y.; Liang, H.; Ueyama, N. *Cryst. Growth Des.* **2008**, *8*(9), 3233.
(16) Lin, H.; Maggard, P. A. *Inorg. Chem.* **2007**, *46*, 1283.
(17) Lin, H.; Yan, B.; Boyle, P. D.; Maggard, P. A. *J. Solid State Chem.* **2006**, *179*, 37.
(18) Luo, J.; Alexander, B.; Wagner, T. R.; Maggard, P. A. *Inorg. Chem.* **2004**, *43*, 5537.
(19) Maggard, P. A.; Yan, B.; Luo, J. *Angew. Chem., Int. Ed.* **2004**, *44*, 2553.
(20) Yan, B.; Capracotta, M. D.; Maggard, P. A. *Inorg. Chem.* **2005**, *44*, 6509.
(21) Lin, H.; Maggard, P. A. *Inorg. Chem.* **2009**, *48*, 8940.
(22) Lin, H.; Maggard, P. A. *Inorg. Chem.* **2008**, *47*, 8044.

Table 1. Single Crystal Data and Structure Refinement Details for Hybrid Solids **1**−**9**

	1	**2**	**3**	**4**
formula	$C_{28}H_{20}AgN_8O_4Re$	$C_{24}H_{18}AgN_6O_5Re$	$C_{12}H_{12}AgN_2O_9Re$	$C_4H_6Ag_2N_6O_8Re_2$
crystal system	triclinic	triclinic	monoclinic	triclinic
space group, Z	$P\bar{1}$, 1	$P\bar{1}$, 2	$P2_1/c$, 4	$P\bar{1}$, 2
temperature, K	296(2)	296(2)	223(2)	296(2)
a, Å	9.7798(5)	8.3697(3)	7.3679(7)	6.3515(3)
b, Å	10.9114(5)	11.6210(4)	26.197(2)	7.7186(3)
c, Å	14.0695(10)	13.5757(5)	9.0160(9)	14.2016(7)
α, deg	102.678(3)	101.646(2)	90.0	89.449(2)
β, deg	105.191(3)	103.515(2)	105.664(5)	81.686(2)
γ, deg	104.828(2)	106.524(2)	90.0	89.229(2)
V, Å^3	1332.96(13)	1178.74(7)	1675.6(3)	688.83(5)
ρ, g/cm	2.059	2.154	2.467	4.119
μ, mm^{-1}	5.324	6.011	8.436	20.367
total reflections	20900	53808	92852	26117
unique reflections	5195	6721	5506	4568
R1, wR2 [$I > 2\sigma(I)$][a]	0.040,0.077	0.027, 0.059	0.037,0.044	0.025,0.050

	5	**6**	**7**	**8**	**9**
formula	$C_{24}H_{30}Ag_6N_{12}O_{27}Re_6$	$C_5H_4AgN_2O_6Re$	$C_{10}H_8Ag_2N_4O_9Re$	$C_{10}H_8AgN_2O_4Re$	$C_{24}H_{24}AgN_4O_4Re$
crystal system	monoclinic	monoclinic	orthorhombic	orthorhombic	orthorhombic
space group, Z	$C2/c$, 4	$P2_1/n$, 4	$Pca2_1$, 4	$Pbca$, 8	$Pnnn$, 2
temperature, K	296(2)	223(2)	173(2)	173(2)	296(2)
a, Å	25.2811(9)	5.7889(3)	22.4400(7)	11.3441(23)	6.3716(3)
b, Å	15.6042(5)	12.2433(6)	5.2048(2)	13.2000(26)	13.1646(5)
c, Å	15.2652(5)	13.6640(6)	13.8475(4)	15.3016(31)	14.8622(6)
α, deg	90.0	90.0	90.0	90.0	90.0
β, deg	117.421(2)	92.2874(18)	90.0	90.0	90.0
γ, deg	90.0	90.0	90.0	90.0	90.0
V, Å^3	5345.4(3)	967.67(8)	1617.33(9)	2291.3(8)	1246.64(9)
ρ, g/cm	3.334	3.310	2.999	2.982	1.936
μ, mm^{-1}	15.757	14.53	9.920	12.272	5.673
total reflections	34966	57306	68948	75390	19042
unique reflections	4699	4781	9247	4139	1148
R1, wR2 [$I > 2\sigma(I)$][a]	0.036, 0.078	0.025,0.033	0.025,0.054	0.046, 0.097	0.052, 0.184

[a] $R_1 = \sum||F_o| - |F_c||/\sum|F_o|$; $wR2 = [\sum w(F_o^2 - F_c^2)^2/\sum w(F_o^2)^2]^{1/2}$; $w = \sigma_F^{-2}$.

Synthesis of $Ag(bpp)_2ReO_4$ (1), $Ag(tpp)ReO_4\cdot H_2O$ (2), $Ag(Hinca)_2ReO_4\cdot H_2O$ (3), $Ag(tro)ReO_4$ (4), $Ag(pda)ReO_4\cdot 1/2H_2O$ (5), $Ag(Hpzc)ReO_4$ (6), $Ag_2(Hpzc)(pzc)(H_2O)ReO_4$ (7), $Ag(bpy)ReO_4$ (8), and $Ag(dpa)_2ReO_4$ (9). **1** was prepared from a reaction of bpp (= 2,3-bis(2-pyridyl)pyrazine) (93.7 mg, 0.40 mmol), Ag_2O (23.2 mg, 0.10 mmol), Re_2O_7 (48.4 mg, 0.10 mmol), and H_2O (0.4 g, 22.2 mmol) as colorless block crystals in ∼30% yield based on Ag. **2** was prepared from a mixture of tpp (= tetra-2-pyridinylpyrazine) (77.6 mg, 0.20 mmol), Ag_2O (23.2 mg, 0.10 mmol), Re_2O_7 (48.4 mg, 0.10 mmol), and H_2O (0.4 g, 22.2 mmol) as yellow bar-shaped crystals in ∼98% yield based on Ag. **3** was prepared from a reaction of Hinca (= isonicotinic acid) (24.6 mg, 0.20 mmol), Ag_2O (11.6 mg, 0.05 mmol), Re_2O_7 (24.2 mg, 0.10 mmol), and H_2O (0.2 g, 11.1 mmol) as colorless bar-shaped crystals in ∼64% yield based on Ag. **4** was synthesized from a reaction of tro (= 1,2,4-triazole) (13.4 mg, 0.20 mmol), Ag_2O (23.2 mg, 0.10 mmol), Re_2O_7 (96.8 mg, 0.20 mmol), and H_2O (0.4 g, 22.2 mmol) as colorless block crystals in ∼76% yield based on Ag. **5** was prepared from a mixture of pda (= pyridazine) (16.0 mg, 0.20 mmol), Ag_2O (23.2 mg, 0.10 mmol), Re_2O_7 (48.4 mg, 0.10 mmol), and H_2O (0.4 g, 22.2 mmol) as colorless plate-shaped crystals in ∼78% yield based on Ag. **6** was synthesized from a reaction of Hpzc (24.8 mg, 0.20 mmol), Ag_2O (23.2 mg, 0.10 mmol), Re_2O_7 (48.4 mg, 0.10 mmol), and H_2O (0.05 g, 2.80 mmol) as colorless bar-shaped crystals in ∼84% yield based on Ag. **7** was prepared from a mixture of Hpzc (= pyrazine-2-carboxylic acid) (59.5 mg, 0.48 mmol), Ag_2O (55.7 mg, 0.24 mmol), Re_2O_7 (58.1 mg, 0.12 mmol), and H_2O (0.2 g, 11.1 mmol) as colorless bar-shaped crystals in ∼80% yield based on Ag. **8** was prepared from a mixture of bpy (= 4,4′-bipyridine) (31.2 mg, 0.20 mmol), Ag_2O (23.2 mg, 0.10 mmol), Re_2O_7 (96.8 mg, 0.20 mmol), and H_2O (0.72 g, 40.0 mmol) as colorless prism crystals in ∼68% yield based on Ag. **9** was prepared from a mixture of dpa (= 1,2-bis(4-pyridyl)-ethane) (73.6 mg, 0.20 mmol), Ag_2O (23.2 mg, 0.10 mmol), Re_2O_7 (48.4 mg, 0.10 mmol), and H_2O (0.3 g, 16.7 mmol) as colorless bar-shaped crystals in ∼70% based on Ag.

Crystallographic Structure Determination of 1−**9.** Suitable single crystals of **1**−**9** were selected and mounted on a nylon loop with a small amount of NVH immersion oil. All X-ray measurements were made on a Bruker-Nonius X8 Apex2 CCD diffractometer using graphite-monochromatized Mo Kα radiation ($\lambda = 0.71073$ Å). The frame integration was performed using the SAINT program.[23] The resulting raw data were scaled and corrected for absorption using a multiscan averaging of symmetry-equivalent data via the SADABS program.[24] Each structure was solved by direct methods and refined by full-matrix least-squares fitting on F^2 using SHELX-97.[25] All non-hydrogen atoms were refined with anisotropic thermal parameters. Hydrogen atoms on the organic ligands were introduced at idealized positions and were allowed to ride on the parent carbon atoms. Details of the crystal parameters, data collections, and structure refinements for all hybrid solids are summarized in Table 1. Selected interatomic distances and angles are listed in Table 2. Further refinement details are provided in the Supporting Information.

Optical Properties. Transmittance spectra for pressed pellets of each powdered sample were measured in a wavelength range

(23) *SAINT+*, version 7.07B; Bruker-Nonius: Madison, WI, 2004.
(24) *SADABS*, version 2.1; Bruker-Nonius: Madison, WI, 2004.
(25) Sheldrick, G.M. *SHELXTL NT, Software Package for Refinement of Crystal Structures*, ver. 5.10; Bruker Analytical X-ray Instruments, Inc.: Madison,WI, 1998.

Table 2. Selected Interatomic Distances (Å) in Hybrid Solids **1**−**9**

atom1	atom2	distance (Å)	atom1	atom2	distance (Å)
		$Ag(bpp)_2ReO_4$ (**1**)			
Ag1	N1	2.431(5)	Re1	O1	1.706(5)
	N4	2.415(5)		O2	1.724(5)
	N5	2.438(5)		O3	1.690(5)
	N7	2.345(5)		O4	1.690(5)
	N8	2.412(5)			
		$Ag(tpp)ReO_4\cdot H_2O$(**2**)			
Ag1	N1	2.469(2)	Re1	O1	1.705(2)
	N2	2.408(2)		O2	1.709(3)
	N4	2.468(2)		O3	1.712(3)
	N5	2.393(2)		O4	1.712(3)
	N6	2.409(3)			
		$Ag(Hinca)_2ReO_4\cdot H_2O$ (**3**)			
Ag1	O6	2.826(3)	Re1	O5	1.710(4)
	O6	2.894(3)		O6	1.723(4)
	N1	2.111(3)		O7	1.710(4)
	N2	2.117(3)		O8	1.721(3)
		$Ag(tro)ReO_4$ (**4**)			
Ag1	O1	2.625(4)	Re1	O1	1.720(3)
	O3	2.690(4)		O2	1.712(3)
	N1	2.146(4)		O3	1.723(3)
	N4	2.155(4)		O4	1.737(3)
Ag2	O5	2.773(4)	Re2	O5	1.730(3)
	O8	2.707(4)		O6	1.720(3)
	N2	2.146(4)		O7	1.719(3)
	N5	2.140(4)		O8	1.738(3)
		$Ag(pda)ReO_4\cdot 1/2H_2O$ (**5**)			
Ag1	O6	2.690(9)	Re1	O1	1.715(7)
	O11	2.802(9)		O2	1.721(8)
	N2	2.179(9)		O3	1.718(9)
	N3	2.177(9)		O4	1.718(9)
Ag2	O2	2.747(9)	Re2	O5	1.713(8)
	O5	2.616(9)		O6	1.724(8)
	O9	2.492(11)		O7	1.708(9)
	N4	2.224(9)		O8	1.712(8)
	N5	2.222(8)	Re3	O9	1.678(11)
Ag3	O1	2.579(8)		O10	1.663(18)
	O6	2.681(9)		O11	1.733(14)
	O8	2.598(8)		O12	1.718(8)
	O9	2.527(12)	Ag1	Ag2	3.575(1)
	N1	2.273(9)		Ag3	3.410(2)
	N6	2.283(9)	Ag2	Ag3	3.557(1)
		$Ag(Hpzc)ReO_4$ (**6**)			
Ag1	O2	2.573(3)	Re1	O3	1.730(2)
	O3	2.648(3)		O4	1.728(2)
	O4	2.842(3)		O5	1.714(2)
	O5	2.552(3)		O6	1.700(2)
	N1	2.284(2)			
	N2	2.249(2)			
		$Ag_2(Hpzc)(pzc)(H_2O)ReO_4$ (**7**)			
Ag1	O1	2.537(2)	Re1	O6	1.728(2)
	O3	2.492(2)		O7	1.721(2)
	O7	2.785(2)		O8	1.727(2)
	N1	2.253(3)		O9	1.722(3)
	N3	2.277(2)	O5−H···O1		2.140(3)
Ag2	O5	2.608(2)	O5−H···O3		2.115(3)
	O6	2.397(2)			
	O8	2.878(2)			
	N2	2.229(3)			
	N4	2.240(3)			
		$Ag(bpy)ReO_4$ (**8**)			
Ag1	O2	3.002(2)	Re1	O1	1.717(2)
	O3	2.869(2)		O2	1.731(2)
	O4	2.954(2)		O3	1.726(2)
	N1	2.141(2)		O4	1.733(2)
	N2	2.132(2)			
		$Ag(dpa)_2ReO_4$ (**9**)			
Ag1	N1	2.316(9)	Re1	O1	1.707(8)

of 200−800 nm at room temperature on a UV−vis spectrophotometer (UV-3600, Shimadzu). To account for the regular reflection losses at the boundary surfaces in the transmittance measurements, each compound was measured twice with two different pellet thicknesses, as detailed previously.[26] Resultant absorption spectra were calculated using the Lambert Law (eq 1) and evaluated as α (cm^{-1}) versus wavelength (nm):

$$\alpha = (1/\Delta x)(\log(1/R_2) - \log(1/R_1)) \quad (1)$$

where α is the absorption coefficient in cm^{-1}; $\Delta x = x_2 - x_1$, where x_1 and x_2 are the thicknesses of the two sample pellets.

X-ray Photoelectron Spectroscopy (XPS). The valence-band XPS spectra were recorded on a RIBER LAS-3000 spectrometer using Mg Kα monochromatized radiation ($h\nu = 1253.6$ eV). The base pressure of the analysis chamber was $\sim 1 \times 10^{-7}$ Torr. Sample sizes were ~1 cm square, and the diameter of the X-ray spot was set at 2−3 mm. The binding energies of the valence-band electronic structures were calibrated by fixing the C 1s core-level peak at 284.8 eV for each sample.

Thermogravimetric Analyses (TGA). The thermal stability and decomposition of the hybrids were measured on a TA Instruments TGA Q50 under flowing nitrogen gas and heating to 500 °C at a programmed rate of 5 °C/min. Weighed amounts (~20 mg) of each hybrid solid were loaded onto Pt pans, equilibrated and tared at room temperature, and the data plotted as the starting weight (%) versus temperature (°C). Post-TGA residuals were characterized by powder X-ray diffraction in transmission mode on an Inel XRG 3000 diffractometer fitted with a CPS 120 position sensitive detector and using Cu $K\alpha_1$ radiation from a sealed tube X-ray source.

Results and Discussion

The structures and properties of Ag(I)−Re(VII) hybrid solids have been systematically investigated by varying the geometry and local coordination sites of the organic ligands, shown in Scheme 1. The resultant hybrid structures are described within separate sections below, and range from 0D (molecules), to 1D (chains), to 2D (layered), and also to interpenetrating 3D (pillar-layered or diamondoid) networks. A listing of all near-neighbor interatomic distances can be found in Table 2 for each of the hybrid structures of **1**−**9**. All symmetry-unique atoms are labeled on at least one representative figure of each structure, a consistent coloring scheme is used, and all hydrogen bonds are drawn as dashed lines. Topological analyses were carried out using TOPOS[27] for structures consisting of extended two- or three-dimensional coordination networks (cutoff distance of ~3.0 Å) and described herein using recently proposed conventional notations.[28]

(26) (a) Kortüm, G.; Haug, P. *Z. Naturforsch.* **1953**, *8a*, 372. (b) Kortüm G. *Reflectance Spectroscopy*; Springer-Verlag: New York, 1969.
(27) Blatov, V. A. *TOPOS, A Multipurpose Crystallochemical Analysis with the Program Package*; Samara State University: Russia, 2004.
(28) Friedrichs, O. D.; O'Keeffe, M.; Yaghi, O. M. *Acta Crystallogr., Sect. A* **2003**, *A59*, 22.

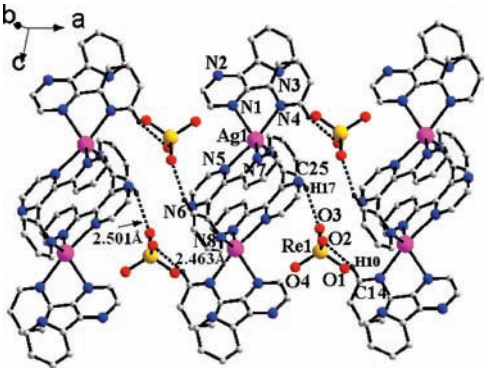

Figure 1. Structural view of **1**, $Ag(bpp)_2ReO_4$, with hydrogen bonds drawn as dashed lines and symmetry-unique atom types labeled. Hydrogen atoms are omitted for clarity.

(i). Monodentate and Multidentate Bridging Ligands Yielding the 0D and 1D Structures of 1, 2, and 3. $Ag(bpp)_2ReO_4$ (1; bpp = 2,3-bis(2-pyridyl)pyrazine). The single crystal X-ray characterization of **1** reveals a molecular (0D) structure that is composed of $[Ag_2(bpp)_4]^{2+}$ dimers that are interconnected via hydrogen bonding to the ReO_4^- anions, that is, C−H···O at ∼2.463(5)−2.501(5) Å (i.e., the − H···O distance throughout the text) down the *a*-axis, as shown in Figure 1. There is only one symmetry-unique Ag site that is coordinated by five nitrogen atoms (Ag−N at 2.345(5)−2.438(5) Å) in a distorted square-pyramidal geometry, twice by two different bpp ligands, and once by a single bpp ligand. Two of the bpp ligands bridge between the two Ag atoms, while the other two bpp ligands are terminating on each Ag, with one of the nitrogen atoms remaining uncoordinated. Each $[Ag_2(bpp)_4]^{2+}$ dimer is hydrogen bonded to four neighboring tetrahedral ReO_4^- anions. The ReO_4^- tetrahedra are nearly regular with Re−O distances of 1.690(5)−1.724(5) Å, with a narrow range of O−Re−O angles from ∼106.9°−111.3°. Two oxygen atoms of each ReO_4^- are hydrogen-bonded to two neighboring $[Ag_2(bpp)_4]^{2+}$ dimers. Thus while the structure of **1** is considered to be molecular based upon the bpp ligand coordination, the weaker hydrogen-bonding interactions lead to some layer-like structural connectivity.

$Ag(tpp)ReO_4\cdot H_2O$ (2, tpp = tetra-2-pyridinylpyrazine). The yellow needle-like crystals of **2** consist of $[Ag(tpp)]_n^{n+}$ chains that are oriented down the *a*-axis, as illustrated in Figure 2. The $[Ag(tpp)]_n^{n+}$ chains are constructed from a single symmetry-unique Ag atom that is coordinated in a distorted square-pyramidal geometry by five nitrogen atoms from three different tpp ligands, at Ag−N distances ranging from 2.393(3)−2.469(3) Å. Each tpp ligand chelates via three nitrogen atoms to Ag, with two other nitrogen atoms bridging to the neighboring Ag sites to form the extended chain. By contrast, previously reported M(I)/tpp (M = Ag, Cu) cationic chains contain three distinct M coordination sites,[29] while the $[Ag(tpp)]_n^{n+}$ chain in **2** consists of just one. The structure of **2** also contains tetrahedral ReO_4^- anions and H_2O molecules that are linked via hydrogen bonds (O1w−H1w···O3, O1w−H2w···O4 at 2.053(3) Å and 2.505(3) Å, respectively) to form a collinear chain. The two chains, $[Ag(tpp)]_n^{n+}$ and $[(ReO_4^-)(H_2O)]_n$, are hydrogen bonded to each other via the oxygen atoms of ReO_4/H_2O and the hydrogen atoms of the tpp ligands at ∼2.32−2.48 Å. Thus, while the Ag coordination geometry is similar to that in **1** with the bpp ligand, the addition of two pyridine groups on the tpp ligand affords the extended bridging coordination in the chains of **2**.

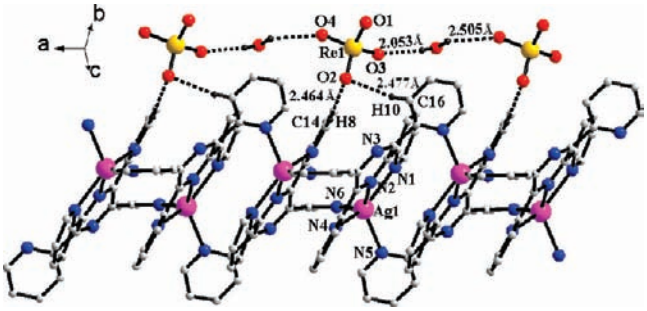

Figure 2. Structural view of **2**, $Ag(tpp)ReO_4\cdot H_2O$, showing the extended $[Ag(tpp)]_n^{n+}$ and $[(ReO_4^-)(H_2O)]_n$ chains aligned down the *a*-axis direction. Hydrogen bonds are drawn as dashed lines with labeled bond distances.

$Ag(Hinca)_2ReO_4\cdot H_2O$ (3; inca = isonicotinate). Shown in Figure 3, the structure of **3** contains dimeric "$Ag_2(inca)_4(ReO_4)_2$" molecular species that are linked to each other via hydrogen bonding interactions. Each Ag atom is coordinated in a slight-distorted seesaw geometry, which is formed by two oxygen atoms (Ag1−O6 at 2.826(3) Å and 2.894(3) Å) from ReO_4^- and two nitrogen atoms (Ag1−N1, −N2 at 2.111(3) Å, 2.117(3) Å, respectively) from two Hinca ligands. The axial N1−Ag1−N2 bond angle is nearly linear, at ∼173.0°, as expected for a seesaw geometry. The carboxylate group of the inca ligand remains uncoordinated to any Ag atoms and must instead be protonated for charge balancing, that is, as Hinca. However, the ReO_4^- anion functions in a bridging role, leading to a relatively close Ag1−Ag1 dimer at 3.4811(7) Å. Within the *bc*-plane, shown in Figure 3B, neighboring Hinca ligands are oriented face-to-face (∼3.75 Å, $\pi-\pi$ interaction) with hydrogen bonding between the carboxylate groups (O−H···O at 2.012(3) Å and 2.091(3) Å). The ReO_4^- anions and uncoordinated water molecules form hydrogen-bonded $[(ReO_4^-)(H_2O)]_n$ zigzag chains (O1w−H···O7, ···O8 at 1.992(2) Å, 2.038(3) Å, respectively) down the *a*-axis. The distances and angles for ReO_4^- are closely similar to **1** and **2**, with Re−O distances of ∼1.710(4)−1.723(4) Å and O−Re−O angles of ∼107.3−111.3°. However, the terminating rather than bridging role of the Hinca ligand results in a molecular structure of "$Ag_2(inca)_4(ReO_4)_2$" dimeric species that are hydrogen bonded to each other and to water.

(ii). Ligands with Neighboring N-Donor Groups Yielding the 2D Structures of 4 and 5. $Ag(tro)ReO_4$ (4; tro = 1,2,4-triazole). The structure of **4** consists of corrugated $[Ag(tro)ReO_4]_n$ layers composed of $[Ag(tro)]_n^{n+}$ zigzag chains that are cross-linked by ReO_4^- anions that coordinate to the Ag sites, as shown in Figure 4. The $[Ag(tro)]_n^{n+}$ zigzag chain consists of two symmetry-unique Ag atoms that alternate down the *b*-axis and are coordinated in a distorted seesaw geometry via the nitrogen atoms of two bridging tro ligands each at Ag−N

(29) (a) Burkholder, E.; Zubieta, J. *Solid State Sci.* **2004**, *6*, 1421. (b) Allis, D. G.; Rarig, R. S.; Burkholder, E.; Zubieta, J. *J. Mol. Struct.* **2004**, *688*, 11.

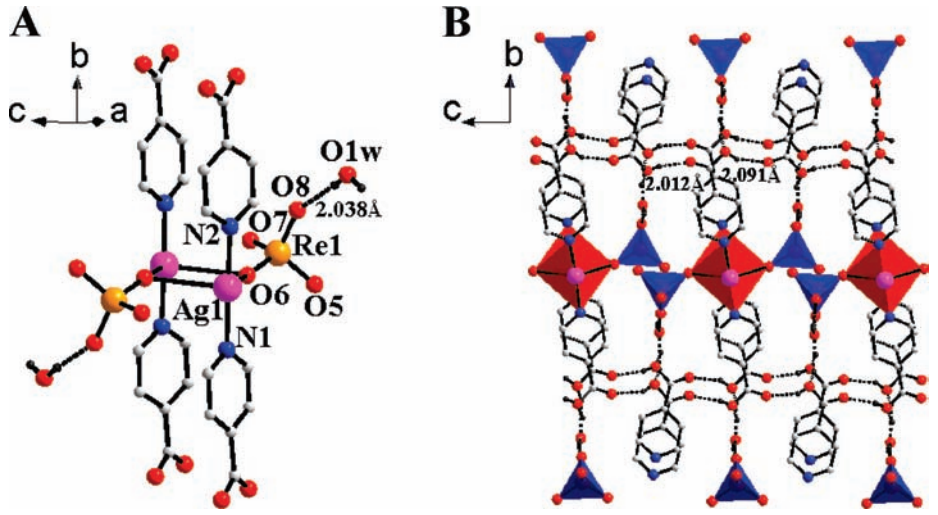

Figure 3. Local (A) and extended (B) structural views of **3**, $[Ag(Hinca)_2ReO_4 \cdot H_2O]$, with all symmetry-unique atoms and hydrogen bonding interactions labeled. The polyhedral view in (B) is aligned down the *a*-axis, with red polyhedra = Ag-centered and blue polyhedra = ReO_4.

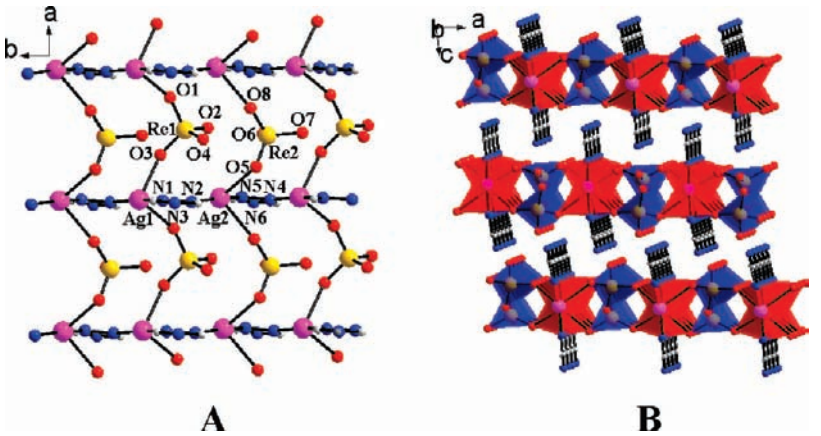

Figure 4. (A) Structural view of a single layer in $Ag(tro)ReO_4$ (**4**) with the symmetry-unique atom types labeled, and (B) an ~[010] polyhedral view of the layers stacked down the *c* axis; Red polyhedra = Ag-centered and blue polyhedra = ReO_4.

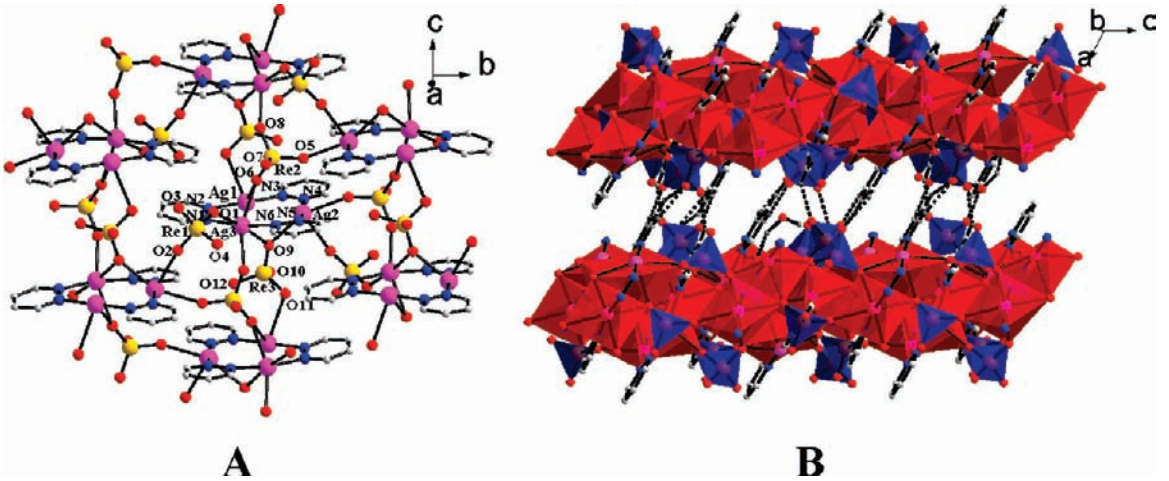

Figure 5. (A) Structural view of a single layer in $Ag(pda)ReO_4 \cdot 1/2H_2O$ (**5**), showing seven trigonal-planar $[Ag_3(pda)_3]^{3+}$ clusters bridged by ReO_4^- anions; (B) An ~[010] polyhedral view of two of these layers stacked in **5** with interlayer hydrogen bonds drawn as dashed lines; Red polyhedra = Ag-centered and blue polyhedra = ReO_4.

distances of 2.140(4)−2.155(4) Å and to two ReO_4^- anions each at Ag−O distances of 2.625(4)−2.773(4) Å. The tro ligands coordinate to the axial sites with a N−Ag−N angle of ~170° and form the backbone of the $[Ag(tro)]_n^{n+}$ zigzag chain. Alternatively, a corrugated "$AgReO_4$" chain can also be described that is oriented

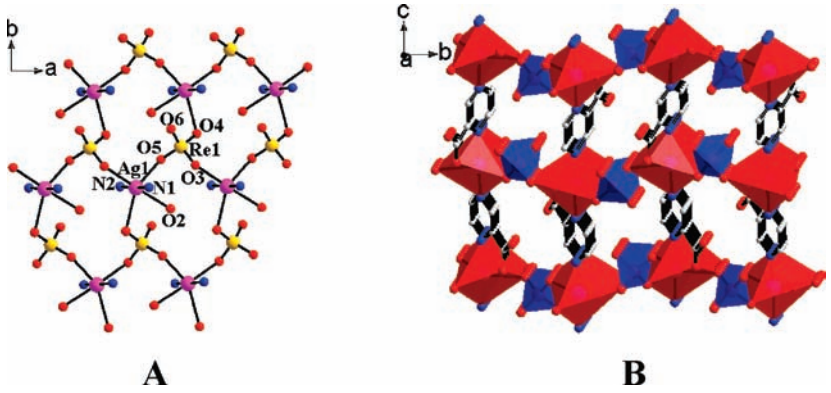

Figure 6. Structural views of Ag(Hpzc)ReO_4 (**6**), showing the (A) "$AgReO_4$" layer with atom types labeled, and (B) an ~[100] polyhedral view. Red polyhedra = Ag-centered and blue polyhedra = ReO_4.

down the *a*-axis and which is cross-linked by the tro ligands. The distorted ReO_4^- tetrahedra exhibit bond angles and distances consistent with the structures previously described above. This layer structure has resulted from the greater number of bridging ReO_4^- anions that serve to cross-link the Ag atoms within a single layer, as compared to the non-bridging ReO_4^- anions in **1** and **2** that result from the chelating and more sterically crowded tpp and bpp ligands.

Ag(pda)$ReO_4 \cdot 1/2H_2O$ (5; pda = pyridazine). The hybrid solid **5** exhibits a layered structure consisting of $[Ag(pda)ReO_4]_n$ layers stacked down the *a*-axis, as shown in Figure 5. This layer is constructed from a remarkable trigonal-planar cluster of three Ag atoms, that is, as a $[Ag_3(pda)_3]^{3+}$ cyclic trimer in Figure 5a, that features a slightly distorted $[Ag_3N_6]$ core with N−Ag−N bond angles between ~170.0°−173.9°. This $[Ag_3(pda)_3]^{3+}$ trimer is unusual but structurally similar to that reported for pyrazolate-bridged Cu^I/Ag^I molecular species,[30] and here represents the first such structural motif synthesized in a hybrid solid. Each $[Ag_3(pda)_3]^{3+}$ cluster is also coordinated to seven bridging ReO_4^- anions that extend the structure in the *bc*-plane to form the $[Ag(pda)ReO_4]_n$ layer.

Including both the N-donor and anionic ReO_4^- ligands, the $[Ag_3(pda)_3]^{3+}$ cluster contains three different Ag coordination geometries, a seesaw (Ag1), a distorted square-pyramidal (Ag2), and a distorted octahedral (Ag3) coordination environment. Each Ag is coordinated to two N atoms on the pda ligands at distances ranging from 2.177(9)−2.283(9) Å, with the differences in coordination geometries owing to the asymmetric arrangement of the ReO_4^- ligands. The Ag1 site is bonded to two oxygen atoms on two ReO_4^- tetrahedra (Ag1−O6, −O11 at 2.690(9) Å and 2.802(9) Å, respectively), to give the seesaw coordination geometry. The distorted square-pyramidal geometry of Ag2 is completed by three oxygen atoms from three ReO_4^- anions (Ag2−O2, −O5, −O9, at 2.747(9) Å, 2.616(9) Å, and 2.492(11) Å, respectively). The Ag3 site is bonded to four oxygen atoms from ReO_4^- anions (Ag3−O1, −O6, −O8, −O9, at 2.579(8) Å, 2.681(9) Å, 2.598(8) Å, and 2.527(12) Å, respectively) and that occupy the equatorial sites of the distorted-octahedral coordination geometry. There are three symmetry-unique ReO_4^- tetrahedra, two of which (Re1 and Re3) are bridging between the Ag atoms on two different $[Ag_3(pda)_3]^{3+}$ clusters, while the other (Re2) is bridging between three neighboring $[Ag_3(pda)_3]^{3+}$ clusters, shown in Figure 5A. Analogous to that described above for **4**, the layered structure of **5** has resulted from the bridging ReO_4^- anions that serve to cross-link the $[Ag_3(pda)_3]^{3+}$ cyclic trimers, as compared to the lower-dimensional structures of **1**−**3** with more ligand-crowded Ag sites and non-bridging ReO_4^- anions.

(iii). Small Asymmetric Bridging Ligands Leading to the Pillar-Layered Structures of 6 and 7. Ag(Hpzc)ReO_4 (6; pzc = pyrazine-2-carboxylate). The structure of **6** is composed of neutral "$AgReO_4$" layers that are cross-linked by Hpzc ligands, shown in Figure 6, with a shortest interlayer distance of ~2.79 Å. A single symmetry-unique "$AgReO_4$" layer stacks down the *c*-axis to generate the full three-dimensional structure in the monoclinic space group $P2_1/n$. Within the layer, there is a single symmetry-unique Ag site that has a distorted-octahedral coordination geometry, with the equatorial positions occupied by one carboxylate group (Ag1−O2 at 2.573(3) Å) and three bridging ReO_4^- anions (Ag1−O3, −O4, −O5, at 2.648(3) Å, 2.842(3) Å, and 2.552(3) Å, respectively). The axial positions are bonded by two nitrogen groups from pzc ligands above and below the layer (Ag1−N1, −N2, at 2.284(2) Å and 2.249(2) Å, respectively), completing the octahedral environment. Each tetrahedral ReO_4^- bridges between three different Ag atoms, with the fourth oxygen vertex located alternately above or below the layer, shown in Figure 6A. A topological analysis of **6** shows that it is classified as a 3,5-c net with 2 nodes (Ag and Re atoms) and the Schläfli symbol $\{6^3\}\{6^9;8\}$.

Each Hpzc ligand chelates to a single Ag atom via the carboxylate and nitrogen groups, and also bridges to a neighboring Ag atom through its opposing nitrogen atom to form the $[Ag(Hpzc)]^+$ chains oriented down the *c*-axis. The Hpzc ligands in a single chain are all oriented in the same direction, while the ligand orientations of neighboring

(30) (a) Raptis, R. G.; Fackler, J. P. *Inorg. Chem.* **1988**, *27*, 4179. (b) Dias, H. V. R.; Polach, S. A.; Wang, Z. *J. Fluorine Chem.* **2000**, *103*, 169. (c) Fujisawa, K.; Ishikawa, Y.; Miyashita, Y.; Okamoto, K. I. *Chem. Lett.* **2004**, *33*, 66. (d) Dias, H. V. R.; Diyabalanage, H. V. K.; Eldabaja, M. G.; Elbjeirami, O.; Rawashdeh-Omary, M. A.; Omary, M. A. *J. Am. Chem. Soc.* **2005**, *127*, 7489. (e) Dias, H. V. R.; Gamage, C. S. P.; Keltner, J.; Diyabalanage, H. V. K.; Omari, I.; Eyobo, Y.; Dias, N. R.; Roehr, N.; McKinney, L.; Poth, T. *Inorg. Chem.* **2007**, *46*, 2979. (f) Yang, G.; Raptis, R. G. *Inorg. Chim. Acta* **2007**, *360*, 2503. (g) Rasika Dias, H. V.; Singh, S.; Campana, C. F. *Inorg. Chem.* **2008**, *47*, 3943.

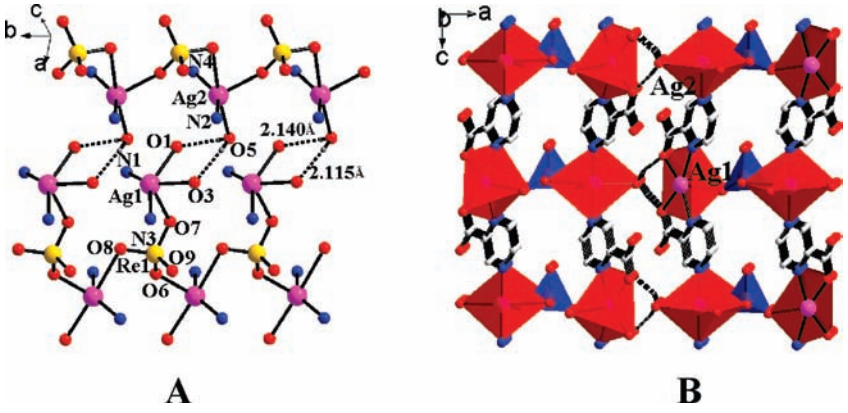

Figure 7. Stuctural views of $Ag_2(Hpzc)(pzc)(H_2O)ReO_4$ (**7**), showing the (A) $[Ag_2(H_2O)ReO_4]_n$ layer with atom types labeled, and (B) an ~[010] polyhedral view with hydrogen bonds as dashed lines; red polyhedra = Ag-centered and blue polyhedra = ReO_4.

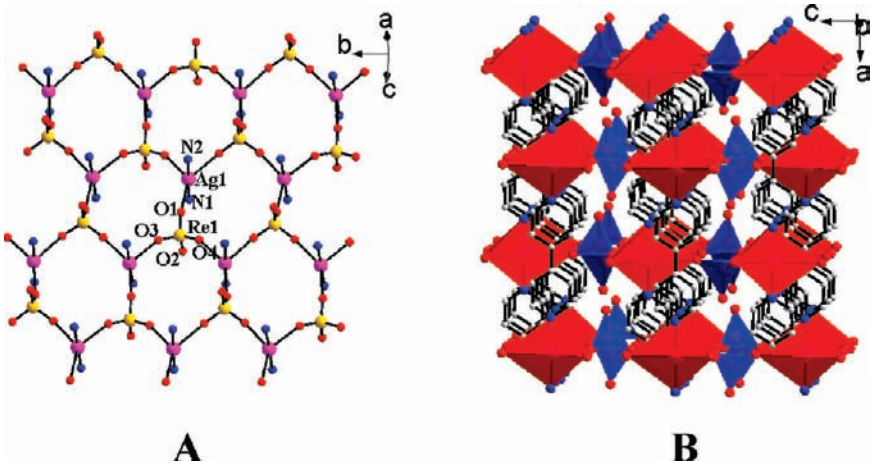

Figure 8. (A) A single "$AgReO_4$" layer of $Ag(bpy)ReO_4$ (**8**) with 6^3 hexagonal nets and all symmetry-unique atom types labeled, and (B) ~[010] polyhedral view of its interpenetrating structure; Red polyhedra = Ag-centered and blue polyhedra = ReO_4.

chains are reversed to cancel any net dipole moment, as required for space group $P2_1/n$. While the carbonyl end (C=O at ~1.21 Å) of the carboxylate group preferentially coordinates to the Ag atom, the alcoholic end (C−OH at ~1.32 Å) remains protonated and uncoordinated. These carboxylate distances are consistent with those of the Hinca ligand of **3** (C=O, C−OH at ~1.22 Å and ~1.34 Å, respectively), that is uncoordinated and protonated as well. Thus, while the terminating Hinca ligand in **3** yields a molecular-type structure, the introduction of a *para* nitrogen group in the Hpzc ligand of **6** results in ligand-bridged "$AgReO_4$" layers. Similar pillared "$AgReO_4$" layers are also found in $Ag(pyz)ReO_4$,[17] showing that the opposing nitrogen atoms on the ligand (sans the carboxylate functionality) are key to forming this type of hybrid structure.

$Ag_2(Hpzc)(pzc)(H_2O)ReO_4$ (7; pzc = pyrazine-2-carboxylate). The structure of **7** is the only one of the nine hybrids described herein to crystallize in a non-centrosymmetric space group, $Pca2_1$. Further, it is the only one with a Ag/Re molar ratio of 2:1 rather than 1:1, as for the other hybrids. Shown in Figure 7, the hybrid structure of **7** is composed of asymmetric $[Ag_2(H_2O)ReO_4]^+$ layers that are stacked down the *c*-axis with pzc/Hpzc ligands bridging between the Ag atoms in each layer, in analogy with the structural role of the Hpzc ligands in **6**. These layers consist of two symmetry−unique Ag sites, distorted square-pyramidal (Ag1) and distorted trigonal-bipyramidal (Ag2) coordination environments that alternate down the $[Ag_2(pzc)(Hpzc)]^+$ chains. Each Ag1 atom is chelated by two nitrogen atoms and two oxygen atoms from two pzc ligands above and below (Ag1−N1, −N3 at 2.253(3) Å and 2.277(2) Å; Ag1−O1, −O3 at 2.537(2) Å and 2.492(2) Å, respectively), and is also coordinated to one oxygen atom from the ReO_4^- anion (Ag1−O7 at 2.785(2) Å). Similarly, Ag2 is coordinated to two pzc ligands through the opposing nitrogen atoms (Ag2−N2, −N4 at 2.229(3) Å and 2.240(3) Å, respectively) and to two ReO_4^- anions via its oxygen atoms (Ag2−O6, −O8 at 2.397(2) Å and 2.878(2) Å, respectively). Additionally, Ag2 is equatorially bonded to one H_2O molecule (Ag2−O5 at 2.608(2) Å) that hydrogen bonds to neighboring carboxylate groups (O5−H···O at ~2.1 Å) shown as dashed lines in Figure 7.

A topological analysis shows that the $[Ag_2(H_2O)ReO_4]^+$ layer in **7** is a new topology with a 3,4-c net with 3 nodes (two Ag and one Re atom) and the Schläfli symbol $\{6;8^2\}\{6^2;8^4\}\{6^2;8\}$. As before for **6**, each tetrahedral ReO_4^- anion bridges between three different Ag sites in **7**, with the fourth oxygen vertice located between the layers in a polar arrangement, shown in Figure 7B. Thus, an undulating $[Ag_2ReO_4]^+$ layer is

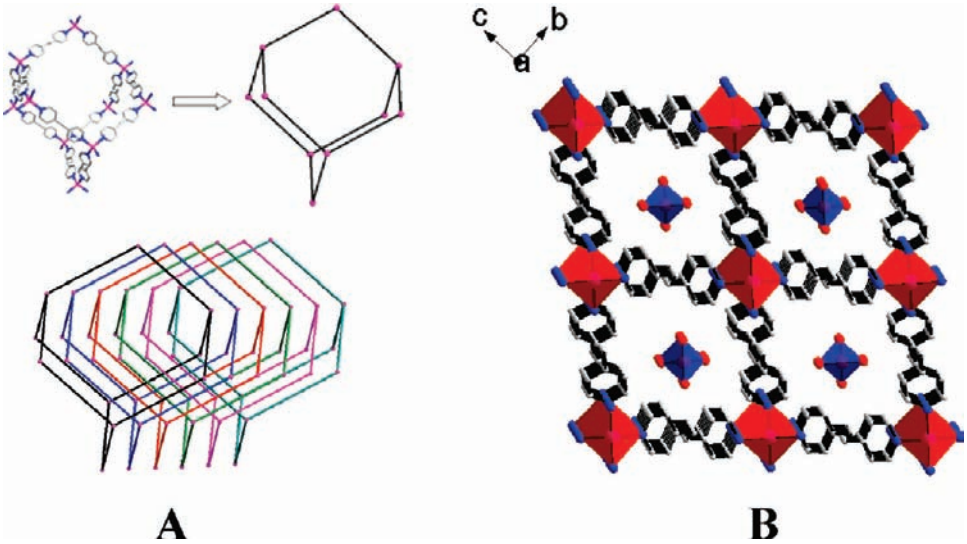

Figure 9. (A) Simplified view of a single diamond-type $Ag(dpa)_2^+$ network, upper, and the 6-fold interpenetration of the same diamond-type net in $Ag(dpa)_2ReO_4$ (**9**), lower. Each node represents a Ag atom. (B) An ~[100] polyhedral view of **9**, with red polyhedra = Ag-centered tetrahedra and blue polyhedra = ReO_4.

formed in **7** that is structurally similar to **6**, but that is Re-deficient owing to the 2:1 (versus 1:1) Ag/Re molar ratio. Further, the layer structure has been able to compensate for this deficiency by incorporating a coordinated water molecule on the same position as the missing ReO_4^- anion.

(iv). Longer Bridging Ligands Yielding the Interpenetrating Structures of 8 and 9. Ag(bpy)ReO_4 (8; bpy = 4,4′-bipyridine). The structure of **8** is a three-dimensional pillar-layered framework that is 2-fold self-interpenetrating, as illustrated in Figure 8 for both a single layer (A) and multiple layers (B). The network is composed of a single symmetry-unique "$AgReO_4$" layer that consists of alternating tetrahedral ReO_4^- anions and Ag-centered trigonal bipyramids that are arranged into 6^3 hexagonal nets and are pillared via the bridging bpy ligands. A topological analysis indicates that the interpenetrating framework of **8** represents a three-dimensional *hms* topology (class IIa) with 3,5-connectivity and a 2-nodal (Re, Ag) net, with the Schläfli symbol $\{6^3\}\{6^9;8\}$. The hybrid network of **8** is iso-structural to that recently reported for $Cu(bpy)ReO_4$,[21] with the replacement of Cu^+ for Ag^+, and thus is described here only briefly.

Within each layer, each ReO_4^- anion bridges via its O vertices to three different Ag^+ in the layer (Ag−O of 2.869(2)−3.002(2) Å), with the fourth vertex oriented either above or below the layer, as found similarly in the silver-rhenate layers of **6** and **7**. The coordination environment of Ag consists of three O atoms from three different ReO_4^- as well as two N atoms from two pyrazine ligands located above and below each layer (2.141(2) Å and 2.132(2) Å for Ag1−N1 and −N2, respectively). The layer-to-layer distance is determined by the length of the bpy ligand at ~7.08 Å, and which allows for intervening layers that interpenetrate through the hexagonal faces of the "$AgReO_4$" net via the bpy ligands. Thus, the bridging role of the bpy ligand in **8** results in a pillared structure similar to that of **6** and **7** (sans the carboxylate group), but the longer ligand length significantly expands the interlayer spacing and results in the 2-fold interpenetration of the pillared network.

$Ag(dpa)_2ReO_4$ (9; dpa = 1,2-bis(4-pyridyl)-ethane). Shown in Figure 9, use of the slightly longer and more flexible dpa ligand in **9** results in a three-dimensional $[Ag(dpa_2)]^+$ diamond-type network that is 6-fold interpenetrating. The structure represents a three-dimensional *dia* topology (class Ia for 6-fold interpenetration) with a 4c-net that is uninodal with the Schläfli symbol $\{6^6\}$. The overall structure is highly symmetric and contains only one symmetry-unique Ag and Re atom. The $[Ag(dpa_2)]^+$ network is constructed from tetrahedrally coordinated Ag via the N donors of four dpa ligands (Ag−N at 2.316(9) Å), Figure 9A. The open channels (dimensions of ~6.1 Å × ~6.1 Å from N1 to N1′) are filled by five other symmetry-related nets as well as the ReO_4^- anionic guests. This network type is relatively common, and has been found for $Cu(bpy)_2ReO_4 \cdot 1/2H_2O$ and for several other metal-organic frameworks.[21,31,32] However, the tetrahedral ReO_4^- anions in **9** are not involved in bridging between the Ag sites, which is their typical role in all other silver(I)-rhenate(VII) hybrids reported herein. The charge-balancing ReO_4^- anions have a much narrower range of tetrahedral Re−O distances (1.701(1) Å) and O−Re−O angles (109.2−109.7°). Thus, use of the longer dpa ligand (versus bpy or pzc in **6** and **8**) results in the only hybrid herein with tetrahedrally coordinated Ag atoms, as compared to the more typical trigonal bipyramidal or seesaw coordination geometries. The absence of ReO_4^- from the Ag coordination environment prevents the formation of any extended Ag−ReO_4 connectivity, as found for hybrids **4**−**8**.

Optical Properties. Measurements of the optical absorption coefficients and bandgap sizes were carried out to investigate the changes arising from the new structural

(31) (a) Blake, A. J.; Champness, N. R.; Chung, S. S. M.; Li, W.-S.; Schroder, M. *Chem. Commun.* **1997**, 1005. (b) Blake, A. J.; Champness, N. R.; Khlobystov, A. N.; Lemenovskii, D. A.; Li, W.-S.; Schroder, M. *Chem. Commun.* **1997**, 1339.

(32) Carlucci, L.; Ciani, G.; Proserpio, D. M.; Sironi, A. *J .Chem. Soc., Chem. Commun.* **1994**, 1325.

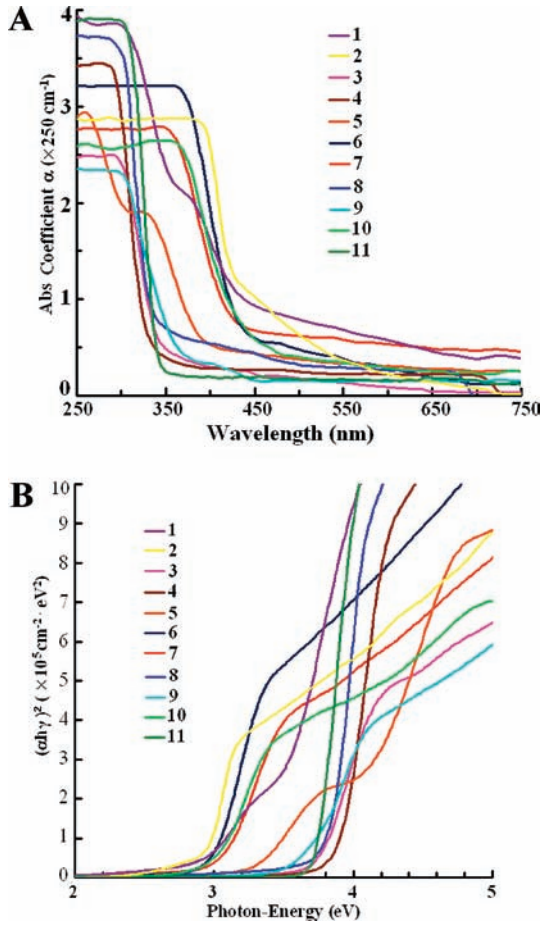

Figure 10. (**A**) A plot of the optical absorption coefficients, α (cm^{-1}) versus wavelength (nm), and (**B**) a plot of $(\alpha h\nu)^2$ vs $h\nu$ for hybrids **1**−**9**, **10** ($AgReO_4$(pyz)), and **11** ($AgReO_4$).

modifications (e.g., coordination environment, network dimensionality, etc.) of the Ag(I)−Re(VII) hybrids. The absorption coefficient, α (cm^{-1}), determines the rate of light absorption in a solid as a function of depth (at α^{-1} the intensity drops to ~36% of its starting intensity). It is one of the most critical but underexplored parameters of semiconductor materials for efficiently capturing solar energy for conversion into fuels and/or electricity; for example, a low α leads to light being poorly absorbed in a material.[33] Generally, semiconductors exhibit a sharp edge in their absorption coefficient spectra, since only light of sufficient energy will excite an electron across the band gap. Thus, α depends on both the solid and on the wavelength of light. As studied previously in $AgReO_4$ and $AgReO_4$(pyz),[17,34,35] the Ag(I)−Re(VII) hybrids are promising candidates for light absorption at relatively low visible-light energies owing to a MMCT excitation between the electron-donating d^{10} (Ag) and electron-accepting d^0 (Re) configurations. Thus, an investigation of their optical properties was conducted herein to probe how the atomic-level structure alters their light-absorption characteristics.

Measurements of α of hybrid solids **1**−**9** were taken on a UV−vis spectrophotometer using transmittance methods in the range of 200−800 nm, and the resultant spectra are plotted as α (cm^{-1}) versus wavelength (nm) in Figure 10A. These spectra include data for the previously reported pillar-layered structure of $AgReO_4$(pyz) (**10**, pyz = pyrazine) and the ligand-free $AgReO_4$ (**11**) for comparison. The measured values of α for these hybrids all fall within one of two different groups, which either exhibit larger bandgap sizes and higher absorption coefficients (**3**, **4**, **5**, **8**, **9**, and **11**) or smaller bandgap sizes in the visible range with lower absorption coefficients (**1**, **2**, **6**, **7**, and **10**). A steep onset of absorption occurs at ~350 nm for the first group and at ~450 nm for the second group. Previous theoretical and experimental studies on Ag(I)−Re(VII) solids have shown that the band-edge absorption occurring at around 340 nm in $AgReO_4$ can be assigned to a MMCT transition ($Ag^{I} \rightarrow Re^{VII}$).[34−36] Further, the shift of the absorption edge by ~0.8 eV to lower energies is consistent with a Ligand-to-Metal Charge Transfer (LMCT) excitation, as was investigated previously in $AgReO_4$(pyz) and $AgReO_4$.[17] Thus, the steep rise in absorption in the first group owes to a MMCT transition, while that of the second group to a LMCT transition.

The optical bandgap size for each of the hybrid solids can be calculated from the respective wavelength-dependent absorption coefficient spectrum. Electronic transition probabilities are given by the following eq 2 when the energy of the photon exceeds the bandgap energy:[37]

$$(\alpha h\nu)^n \propto (h\nu - E_g) \qquad (2)$$

where α is the absorption coefficient (cm^{-1}), $h\nu$ is the photon energy (eV), E_g is the band gap energy (eV), and $n = 2$ when the transition is direct, and $n = 1/2$ when the transition is indirect. Bandgap sizes (E_g) can be estimated from the linear portion of the plots of $(\alpha h\nu)^n$ versus $h\nu$ when extrapolating to zero. The plots of $(\alpha h\nu)^2$ versus $h\nu$, shown in Figure 10B, yield bandgap sizes that are consistent with the observed colors and also suggest that each of the lowest energy excitations are direct. The calculated bandgap sizes for each compound are 2.89 eV (**1**), 2.60 eV (**2**), 3.70 eV (**3**), 3.75 eV (**4**), 3.30 eV (**5**), 2.90 eV (**6**), 2.96 eV (**7**), 3.71 eV (**8**), 3.46 eV (**9**), 2.91 eV (**10**; $AgReO_4$(pyz)), and 3.68 eV (**11**; $AgReO_4$). Hybrid solids in the group with the higher values of α show a range of bandgap sizes from ~3.30−3.75 eV, while those in the second group with lower values of α show a range of bandgap sizes from ~2.60−2.96 eV. For hybrids in the former group, that is, **3**, **4**, **5**, **8**, **9**, **11** assigned to a MMCT excitation, there is a close correlation of α with the Ag−ReO_4 network dimensionality but not with the bandgap size. For example, as α decreases in the order of **11** > **8** > **4** > **5** > **3** > **9**, the network dimensionality of Ag−ReO_4 (minus the ligand) decreases from 3D condensed (**11**) to 2D layers (**8**, **4**, **5**) to 0D molecular (**3**) and to no connectivity (**9**). The ligands have a predominant role in altering the Ag−ReO_4 network

(33) Honsberg C.; Bowden, S.; *Photovoltaics CDROM, II ed.*, **2008**.
(34) Kunkely, H.; Vogler, A. *Inorg. Chim. Acta* **2004**, *357*, 1317.
(35) Otto, J. W.; Vassiliou, J. K.; Porter, R. F.; Ruoff, A. L. *J. Phys. Chem. Solids* **1992**, *53*, 631.
(36) Spitaler, J.; Ambrosch-Draxal, C.; Nachbauer, E.; Belaj, F.; Gomm, H.; Netzer, F. *Phys. Rev. B* **2003**, *67*, 115127/1.
(37) (a) Bube, R. H. *Electrons in Solids*; Academic Press, Inc.: San Diego, 1988; (b) Van Leeuwen, R. A.; Hung, C. J.; Kammler, D. R.; Switzer, J. A. *J. Phys. Chem.* **1995**, *99*, 15247.

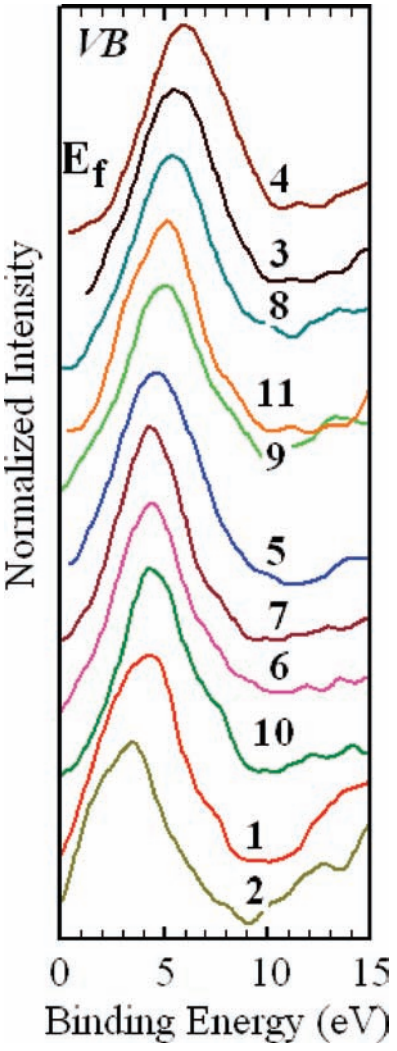

Figure 11. XPS valence-band spectra of hybrids **1**−**9**, **10** ($AgReO_4$-(pyz)) and **11** ($AgReO_4$), ordered according to decreasing binding energies.

dimensionality, and thus, the absorption coefficients that are dependent on the electronic transition probabilities.

X-ray Photoelectron Spectroscopy (XPS). Electronic structure calculations on Ag(I)/Cu(I)-Rhenate(VII) hybrids have shown previously that the conduction band is composed primarily of unfilled Re 5d orbitals, while the valence band originates from mixture of Ag 4d, O 2p, and N 2p orbitals. As described above, the ReO_4^- anions in hybrid structures **1**−**9** exhibit nearly identical tetrahedral coordination geometries, while the coordination environments and connectivities of the Ag sites vary substantially as a result of the different ligands. Thus, while the valence bands are expected to exhibit a larger variation in energies, the conduction bands are more fixed at similar energy levels.

The XPS results show that the valence band energies of the hybrids, shown in Figure 11, closely correlate with the changes in their bandgap energies (E_g) (central peak positions arranged from smallest to largest E_g: **2**, 3.85 eV; **1**, 4.40 eV; **10**, 4.45 eV; **6**, 4.50 eV; **7**, 4.52 eV; **5**, 4.80 eV; **9**, 4.95 eV; **11**, 5.10 eV; **3**, 5.18 eV; **8**, 5.20 eV; **4**, 5.45 eV). For example, the highest valence band energy was measured for **2** which has the lowest E_g of 2.60 eV, followed by **1**, **10**, **6**, and **7** with the next highest E_g sizes that range from ~2.89−2.96 eV. The next lowest set of valence band energies for **5**, **9**, **11**, **8**, **3** and **4** also closely follows the same trend toward increasing E_g from ~3.30−3.75 eV. Owing to the nature of the bandgap transition, that is, LMCT for the first five hybrids and MMCT for the next six, the valence band is composed primarily of the Ag d-orbitals in the latter and the ligand-based π-orbitals in the former. Obviously, there is significant orbital mixing between the Ag 4d and ligand π-orbitals and a gradual progression of their mixture in the valence band, and both are significant factors in determining the resultant E_g of the hybrids.

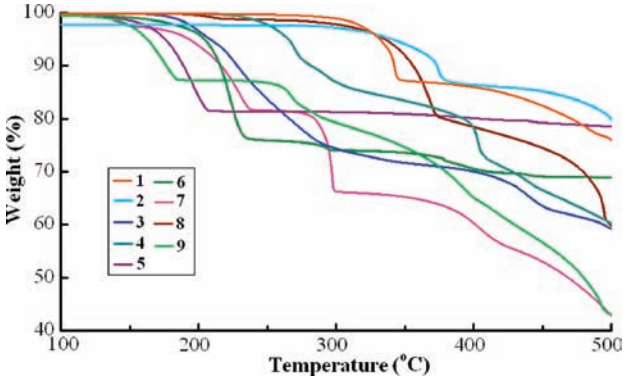

Figure 12. Thermogravimetric analyses (TGA) of hybrids **1**−**9**, plotted as weight (%) versus temperature (°C).

The hybrid network dimensionality (e.g., clusters, chains) and local coordination environments should effect the bandgap sizes, such as via the strength of the d-orbital-to-ligand interactions or in the band broadening for extended versus molecular networks. Described above, the local Ag coordination environments vary quite significantly among the hybrids **1**−**9**, and are dependent on the N-donor positions, the presence of carboxylate groups, and the geometry and size of the ligand. These include a distorted seesaw $\{AgN_2O_2\}$ coordination geometry in **3** and **4**, a distorted $\{AgN_4\}$ tetrahedral geometry in **9**, a distorted $\{AgN_2O_4\}$ octahedral geometry in **6**, and distorted $\{AgN_5\}$ or $\{AgN_2O_3\}$ square pyramidal or trigonal bipyramidal coordination geometries in **1**, **2**, **7**, **8**, and **10**. The structure of **5** contains Ag-centered seesaw, octahedral, and square-pyramidal coordination geometries. The greater d-orbital interactions of the distorted square-pyramidal/trigonal-bipyramidal and octahedral coordination geometries in **1**, **2**, **6**, **7**, and **10** raise the filled Ag $4d^{10}$ orbitals to higher energies and results in their relatively smaller bandgap sizes. By comparison, the tetrahedral and seesaw coordination geometries of **3**, **4**, **9**, and **11** result in weaker d-orbital interactions, a lower-energy valence band, and increased bandgap sizes. By contrast, no trends were found between the Ag−ReO_4 network dimensionality and the bandgap sizes, owing to the relatively much weaker interaction between the Re 5d-orbitals and the Ag- or ligand-based orbitals.

Thermogravimetric Analysis (TGA). Many hybrid metal-oxides/organics exhibit high thermal stabilities, can be thermally converted to new or known condensed phases after removal of the ligand, and reversibly absorb water or other small molecules. The TGA results for hybrid solids **1**−**9** are shown in Figure 12. The post-TGA products were characterized using Powder X-ray Diffraction (PXRD)

and these results provided in the Supporting Information (Figure 2S). The TGA results can be separated into two groups, one group (**1**, **2**, **8**, and **9**) that decomposes into Ag(s) and other amorphous solids, and another group that decomposes to yield the condensed $AgReO_4$ (**4**, **5**, **6**, and **7**) or the ReO_2 (**3**) phase.

In the first group, the strongly chelating bpp and tpp ligands in **1** and **2** produce two of the most thermally stable hybrid structures at temperatures of up to ~300−350 °C. Further, heating to ~500 °C results in a weight change corresponding to only a partial loss of the ligands (~20.2%, calcd. 56.7% for **1**; ~21.8%, calcd. 50.8% for **2**), although the lattice H_2O in **2** is easily removed at ~100 °C (~2.3%, calcd. 2.4%). Both post-TGA residuals contain a similar mixture of Ag(s) and an amorphous material. The same residual products were found for **8** and **9** as well, with the bridging bpy and dpa ligands. In **8**, removal of the bpy ligand begins at ~300 °C and extends to ~480 °C, while the removal of the dpa ligand in **9** extends from ~150 to ~480 °C. The thermal stability of **9**, which is lower than any of the other hybrids, is because of the absence of any close Ag−ReO_4 interactions. Thus, all of the larger and chelating ligands (bpp, tpp, bpy, and dpa) inhibited the soft collapse of the metal-oxide framework, and instead yielded Ag(s) and amorphous products rather than crystalline $AgReO_4$.

In the second group, the thermal decomposition of hybrids **5**, **6**, and **7** leads to the low temperature loss of their respective pda and pzc ligands at ~200−250 °C and the formation of condensed $AgReO_4$. Interestingly, while this transformation occurs in a single weight-loss step for **5** and **6**, the weight loss of **7** exhibits four distinct steps. On heating **7** to ~500 °C, an ~2.4% weight loss of coordinated water from 120−160 °C (calcd. 2.5%) occurs, followed by an ~16.7% weight loss at ~160−240 °C that corresponds to the removal of one pzc ligand per formula (calcd. 16.9%), and followed by another ~16.8% weight loss of the remaining pzc ligand at ~280−300 °C, resulting in the formation of $AgReO_4$ and Ag. The intermediate products are unknown and have not yet been structurally characterized. The fourth and last weight loss for **7** at > 400 °C is due to the decomposition of $AgReO_4$. The post-TGA products of **4** were also determined to be a mixture of $AgReO_4$ and Ag, with the loss of tro ligands from ~220−360 °C (~16.9%, calcd. 16.2%). Lastly, the decomposition of **3** exhibits two weight-loss steps of ~41% extending from 180 to 500 °C, and that corresponds to the loss of both lattice water and inca ligands (calcd. 42.5%), yielding a mixture of Ag and ReO_2. Thus, all of the shorter ligands (tro, pda, and pzc) resulted in a soft collapse of the hybrid structures to give $AgReO_4$ in the products.

Conclusions

A series of nine new silver(I)-rhenate(VII) oxide/organic hybrids was synthesized. The use of large multidentate chelating ligands resulted in the molecular and chain-like structures of Ag(bpp)ReO_4 and Ag(tpp)$ReO_4 \cdot H_2O$ with limited Ag−ReO_4 connectivity. Conversely, shorter bridging ligands yielded the layered and pillared-types of hybrid structures of Ag(tro)ReO_4, Ag(pda)$ReO_4 \cdot 1/2H_2O$, Ag(Hpzc)ReO_4, and Ag_2(Hpzc)(pzc)$(H_2O)ReO_4$, respectively, each with a two-dimensional Ag−ReO_4 connectivity. Lastly, the interpenetrating networks of Ag(bpy)ReO_4 and Ag$(dpa)_2ReO_4$ are found with the longest bridging ligands. Measured bandgap sizes show that the hybrid solids fall into two groups, and exhibit either larger bandgap sizes of ~3.30−3.75 eV owing to MMCT excitations, or smaller bandgap sizes of ~2.60−2.96 eV from LMCT excitations. For the hybrid group with the larger bandgap sizes and MMCT, the absorption coefficients are relatively larger and closely correlate with the Ag−ReO_4 network dimensionality. The XPS spectra reveal that the bandgap sizes are primarily determined by changes in the valence band energies that are a function of the Ag coordination geometries and d-orbital energies. TGA results reveal the highest possible thermal stability of ~300 °C for Ag(bpp)ReO_4, Ag(tpp)$ReO_4 \cdot H_2O$, and Ag(bpy)ReO_4, while for the smaller ligands in Ag(tro)ReO_4, Ag(pda)$ReO_4 \cdot 1/2H_2O$, and Ag(Hpzc)ReO_4 there is a lower-temperature structural collapse to yield condensed $AgReO_4$. In summary, the nature of the coordinating ligand plays a critical role in directing the structure of each hybrid, and therefore can be of great utility in tuning their optical properties in the future design of new materials for solar-energy conversion.

Acknowledgment. The authors acknowledge support of this research from the donors of the American Chemical Society Petroleum Research Fund (#46803-AC10), and from the Chemical Sciences, Geosciences and Biosciences Division, Office of Basic Energy Sciences, Office of Science, U.S. Department of Energy (DE-FG02-07ER15914), and also assistance with the collection of single crystal X-ray data (P. Boyle).

Supporting Information Available: Crystallographic data for **1**−**9** in CIF format, tables of atomic coordinates and equivalent isotropic displacement for each compound, powder X-ray diffraction results for all prepared compounds including for the as-synthesized hybrids and post-TGA residuals. This material is available free of charge via the Internet at http://pubs.acs.org.